Materials & Design 205 (2021) 109697

Contents lists available at ScienceDirect

Materials & Design

journal homepage: www.elsevier.com/locate/matdes

# An accelerated creep assessment method based on inelastic strain partitioning and slow strain rate testing

V. Norman *, M. Calmunger

*Division of Engineering Materials, Department of Management and Engineering, Linköping University, SE-58183 Linköping, Sweden*

ARTICLE INFO

*Article history:*
Received 27 January 2021
Revised 19 March 2021
Accepted 30 March 2021
Available online 20 April 2021

*Keywords:*
Creep
Slow-strain-rate testing
Stress relaxation
Constitutive behaviour
Metallic material

ABSTRACT

A new accelerated creep assessment method to evaluate the creep performance of metals and alloys from high-temperature tensile tests, *i.e.* slow-strain-rate testing (SSRT), is proposed and evaluated. The method consists of decomposing the inelastic strain into a plastic and creep component by adopting general assumptions on the inelastic strain behaviour of materials, formulated using a state variable formalism and verified by tensile tests with intermediate dwell times at constant stress. Either, the plastic and creep strain components are considered non-interacting and additive, as observed in the stainless steel AISI 316L at 600 °C. Or, as in the case of the ductile cast iron EN-GJS-SiMo5-1 at 500 °C and the nickel-base superalloy Hastelloy X at 800 °C, the components are considered unified, meaning that the effect of inelastic straining is the same irrespective of whether it is caused through creep at constant stress or by plastic deformation due to an instantaneous stress increase. Based on these assumptions, the proposed method is used to assess the creep strain from SSRT in good agreement with conventional creep test results.
© 2021 The Authors. Published by Elsevier Ltd. This is an open access article under the CC BY license (http://creativecommons.org/licenses/by/4.0/).

## 1. Introduction

Creep deformation is the time-dependent and often undesirable inelastic deformation which can occur in structural materials at elevated temperatures despite being in a state of mechanical equilibrium. Creep deformation is considered detrimental since it is associated with geometric distortions and redistributions of stress [1], which over time, might contribute to loss in operation functionality or complete malfunction. On top of this, microscopic damage accumulation has been explicitly related to the creep deformation in metallic materials [2–4]. For these reasons, the creep phenomenon is of importance in mechanical design of load-bearing structures exposed to high temperatures, such as in heavy-vehicle automotive components [5,6], aero engines [2,7,8] and the power generation industry [9,10]. Common to these industries, they seek to increase the operation temperature since this generally translates into reduced fuel consumption and emissions [6,8–10]. Thus, along with other aspects such as high-temperature oxidation and fatigue performance, the resistance to creep deformation is of critical importance to the ongoing material development driven by the urge to reach efficiency and emission objectives.

More precisely, creep is usually defined as the inelastic strain accumulated at applied constant stress at a constant temperature for a given material, which can be measured following standard procedures, *i.e.* a uniaxial creep test [11]. Uniaxial creep testing is a natural part of material characterization of materials intended for high-temperature operation, *e.g.* austenitic stainless steels [12,13], ductile cast iron [14,15] and nickel-base superalloys [16–18], and the acquired creep data is commonly used in material design, see for instance [13,16,19]. However, creep testing is a time-consuming test procedure, especially if low stress levels are of interest. As a consequence, many alternative accelerated creep assessment methods have been proposed over the years, such as extrapolation methods [20–23], methods based on stress-relaxation testing [24,25], *i.e.* the application of a constant uniaxial strain while measuring the decrease in uniaxial stress, and methods based on tensile testing [15,26–32].

To assess creep strain based on high-temperature tensile testing, commonly referred to as slow-strain-rate testing (SSRT) in this context, two different types of approaches have been considered. Either, it is based on the observation of the correspondence between a saturated tensile test, *i.e.* when the stress-strain slope approaches zero, and conventional constant-stress creep tests [15,26–29]. The approach is motivated by the experimentally observed agreement when comparing steady-state creep strain rates as a function of creep stress with the tensile-test strain rate

* Corresponding author.
*E-mail address:* viktor.norman@liu.se (V. Norman).

https://doi.org/10.1016/j.matdes.2021.109697
0264-1275/© 2021 The Authors. Published by Elsevier Ltd.
This is an open access article under the CC BY license (http://creativecommons.org/licenses/by/4.0/).

as a function of the ultimate tensile strength [27,29]. Alternatively, the second approach consists of fitting a creep constitutive law, *e.g.* Norton creep law, to the SSRT test and evaluate the creep strain based on the fitted parameters [30–32]. However, both approaches have their limitations. In particular, the former approach is not applicable if the material manifests significant hardening such that saturation is never attained, which is likely for low-temperature tests [26]. Whereas for the second approach, the assessment will depend on the particular choice of creep constitutive equation, which do not take unanticipated creep phenomena into consideration, if not accounted for in the fitted model.

An alternative and unexplored approach to assess creep based on tensile testing is by inelastic strain partitioning which starts from the assumption that the uniaxial inelastic strain $\varepsilon_{in}$ in a tensile test may be decomposed into a creep and plastic component, $\varepsilon_{cr}$ and $\varepsilon_{pl}$, as

$$\varepsilon_{in} = \varepsilon_{cr} + \varepsilon_{pl} \tag{1}$$

where the creep strain $\varepsilon_{cr}$ is the part of the inelastic strain having an explicit time dependence, in parity with the inelastic strain accumulated under constant-stress conditions. However, whereas the total inelastic strain $\varepsilon_{in}$ can be evaluated at any instant during a SSRT test by subtracting the elastic strain from the total mechanical strain, the two strain components are unknown on beforehand. Therefore, additional considerations are required, such as to determine whether the accumulation of in one inelastic strain component affects the accumulation of the other. Even though the interaction may be arbitrary and material dependent, relatively simple considerations of the inelastic strain, such as viewing the creep and plastic strain completely decoupled and independent [33–36], or oppositely, as indistinguishable and unified quantities [33,37–41], have shown to provide an accurate description of the high-temperature behaviour of many engineering alloys. Thus, it is reasonable to suggest that simple and general assumptions regarding inelastic strain partitioning can provide means to assess creep at load conditions other than constant-stress conditions through Eq. 1.

Accordingly, the purpose of the present investigation is to develop and evaluate a new accelerated creep assessment method intended for material development, based on inelastic strain partitioning and SSRT. For this purpose, a theoretical basis for inelastic strain partitioning is established in terms of well-known state-variable modelling concepts, on which a methodology to assess uniaxial creep strain and strain rate using SSRT data is based. By comparison to conventional uniaxial creep and stress relaxation tests on a wide set of materials, it is demonstrated that the proposed methodology provide estimates in good agreement. Thus, as an outcome of the present investigation, SSRT is justified as a complementary accelerated method to uniaxial creep testing, which can be used to quickly evaluate and compare the creep performance of high-temperature alloys for material design and development. In particular, the main advantages are the greater availability of tensile test data and the necessary laboratory equipment, as well as that creep and standard mechanical properties assessment can be done on the same test data set, thereby reducing the need of resource-intense creep testing.

## 2. Accelerated creep assessment method by inelastic strain partitioning

In this section, the proposed method based on inelastic strain partitioning to assess the creep deformation is presented. For this purpose, two inelastic strain partitioning assumptions are formulated based on previous observations of two general inelastic strain behaviours in metallic materials, here denoted as a decoupled and unified inelastic strain partitioning, in Section 2.1. Based on these partitioning principles, a methodology is proposed to assess the creep strain and the corresponding creep strain rate by SSRT testing in Section 2.2.

### 2.1. Theory of inelastic strain partitioning

#### 2.1.1. State variable formalism

For a general and phenomenological analysis of deformation, an local-equilibrium thermodynamic formalism, or state variable modelling, is considered [42–46]. Following this theory, the current state of the material occupying an infinitesimal volume element, including the amount of deformation, hardening state, damage or any other kind of relevant information, is represented by a set of mutually independent state variables. The state variables are divided into observables, *i.e.* variables which can be observed and regulated experimentally, and internal or hidden variables, which by definition cannot be explicitly affected. Instead, they are dependent on the observables through evolution laws. Importantly, the material state is uniquely determined by the set of state variables, which represents an equilibrium state in the thermodynamic sense.

For the present purpose, the observables are taken as the Cauchy stress tensor $\sigma_{ij}$, as will be motivated later, and the temperature $T$. The initially unknown internal variables are denoted as $v_\gamma$ where $\gamma = 1, 2, ..$ is the index over all finite-numbered internal variables which influence the material state. It must be noted that each internal variable can be of different mathematical nature, *i.e.* either a scalar, vector or a high-order tensor. As mentioned, the internal variables depend on the observables according to an evolution law usually expressed by a differential

$$dv_\xi = \mathscr{M}_{\xi ij}(\sigma_{kl}, T, v_\gamma)d\sigma_{ij} + \mathscr{N}_\xi(\sigma_{kl}, T, v_\gamma)dT \tag{2}$$

using the Einstein index summation convention, and where $\mathscr{M}_{\xi ij}$ and $\mathscr{N}_\xi$ are functions dependent on the current state of the material as represented by the state variables.

By proper selection of internal variables and evolution laws, most material constitutive behaviours observed experimentally may supposedly be simulated. However at this point, the formalism does not incorporate explicit time-dependencies since a change in state is only achieved by altering the observables, irrespective of the time frame. Thus, in order to include time-dependent effect such as creep, Eq. 2 is adjusted to

$$dv_\xi = \mathscr{M}_{\xi ij}(\sigma_{kl}, T, v_\gamma)d\sigma_{ij} + \mathscr{N}_\xi(\sigma_{kl}, T, v_\gamma)dT + \mathscr{F}_\xi(\sigma_{kl}, T, v_\gamma)dt \tag{3}$$

where $\mathscr{F}_\xi$ is a function of the state variables and $dt$ is an infinitesimal time increment. From this expression, we see that the internal variables may evolve both due to a change in the observables, but also due to the elapse of time even when the observables are kept fixed, *i.e.* when $d\sigma_{ij} = 0$ and $dT = 0$. This expression is the same as derived by [45], which is a special case of the more general theory by [43], who also considered the rate of the state variable as independent variables.

#### 2.1.2. Inelastic strain under isothermal uniaxial load conditions

In the current investigation, SSRT load conditions are of concern, *i.e.* under isothermal condition, $dT = 0$, and when uniaxially loaded, that is $\sigma_{ij} = \sigma$ when $i = j = 1$ and 0 otherwise. In this case, Eq. 3 is reduced to

$$dv_\xi = \mathscr{M}_\xi(\sigma, v_\gamma)d\sigma + \mathscr{F}_\xi(\sigma, v_\gamma)dt \tag{4}$$

where the uniaxial inelastic strain $\varepsilon_{in}$ is identified as one of the internal variables, defined as

$$\varepsilon_{in} = \varepsilon - \varepsilon_{el} \tag{5}$$

where $\varepsilon$ is the uniaxial strain and $\varepsilon_{el}$ is the uniaxial elastic strain recovered if instantaneously unloaded to zero stress. Thus, by Eq. 3

$$d\varepsilon_{in} = \mathscr{H}^{-1}(\sigma, \varepsilon_{in}, v_\gamma)d\sigma + \mathscr{A}(\sigma, \varepsilon_{in}, v_\gamma)dt \tag{6}$$

where $v_\gamma$ now represent the rest of the internal variables, and $\mathscr{H}^{-1}$ and $\mathscr{A}$ are functions specifically associated with the inelastic strain.

It is now convenient to motivate why stress is selected as an observable and not the uniaxial strain. To see this, the following definitions of uniaxial plastic and creep strain are adopted,

$$d\varepsilon_{pl} = \mathscr{H}^{-1}(\sigma, \varepsilon_{pl}, \varepsilon_{cr}, v_\gamma)d\sigma \tag{7}$$

$$d\varepsilon_{cr} = \mathscr{A}(\sigma, \varepsilon_{pl}, \varepsilon_{cr}, v_\gamma)dt \tag{8}$$

where the dependency on $\varepsilon_{in}$ has been generalised to a separated dependency on $\varepsilon_{pl}$ and $\varepsilon_{cr}$. By this definition, creep strain is defined as the inelastic strain accumulated when the stress is constant, which is in agreement with how standard creep tests are interpreted.

It must be emphasised that by this formalism, Eq. 7 governs the inelastic strain response at high load rates for which creep straining is negligible due to insufficient time, since

$$d\varepsilon_{in} = d\varepsilon_{pl} + d\varepsilon_{cr} \cong \mathscr{H}^{-1}(\sigma, \varepsilon_{pl}, 0, v_\gamma)d\sigma \tag{9}$$

when $\dot{\sigma}$ is large. Thus, performing tensile tests with increasing load rate should indicate a convergence to a unique rate-independent stress-strain curve, which will be discussed in Section 4.2.

### 2.1.3. Inelastic strain partitioning assumptions

Two special cases of Eqs. 7 and 8 in accordance with general and frequently employed descriptions of the inelastic strain behaviour of metallic materials will no be formulated. In the first case, the plastic and creep strain components are assumed to be independent and additive, here denoted as decoupled inelastic strain. Successful description by constitutive modelling based on decoupled inelastic strain has been reported for many engineering alloys [33–36]. Regarding the second case, plastic and creep strain components are considered unified, meaning that the effect of inelastic strain on the material is the same regardless of whether it is accumulated as creep strain at constant stress or as plastic strain by instantaneous loading. In fact, the unified description of inelastic strain has been used extensively in constitutive modelling of metallic materials at high temperatures [33,37–41].

An instructive test to analyse the inelastic strain behaviour of materials is to perform a high load-rate tensile test with an intermediate constant-stress dwell time and investigate the effect of the dwell time on the subsequent hardening behaviour [47–50]. In particular, such a test provides information regarding eventual coupling effects due to the dwell time, when compared to a tensile test without intermediate dwell. Fig. 1 illustrates the expected response of the two ideal inelastic strain behaviours when subjected to such test conditions. Accordingly, a unified inelastic strain is expected to manifest a convergence between the load segment ensuing the dwell period and the stress-strain curve without dwell, connected by an elastic load segment, as indicated in Fig. 1. Because the creep strain accumulated during the dwell time is defined such that it causes the same hardening effect as an instantaneous plastic strain would have done, the curves must coincide. In contrast, the load segment after the dwell period for decoupled inelastic strain behaviour should not return to the no-dwell curve, see Fig. 1. Rather, the former curve is translated in the horizontal direction as prior creep strain must leave the hardening state unaffected and therefore shifts the curve in the positive strain direction.

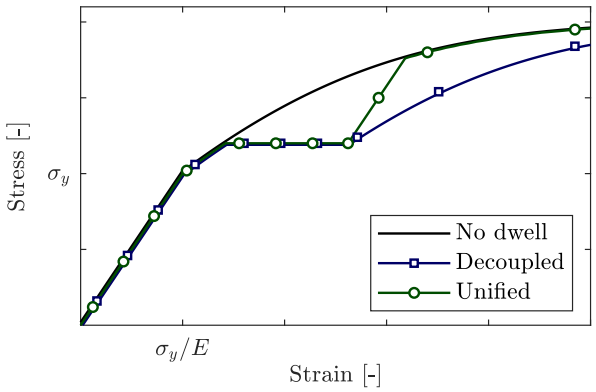


**Fig. 1.** Comparison of decoupled and unified inelastic strain behaviour when subjected to a high load-rate tensile test with an intermediate constant-stress dwell time, where the line without markers represents the stress-strain curve when loaded without an intermediate dwell time.

*2.1.3.1. Decoupled inelastic strain.* In this case, the plastic and creep are defined to be additive and independent, meaning that accumulation of plastic strain does not influence creep strain and vice versa. Furthermore, it is also specified that the creep strain is the only internal variable which is explicitly time-dependent, *i.e.* aspects such as hardening do not change with time if the observables are kept constant. Mathematically, the decoupled inelastic strain behaviour is formulated as

$$d\varepsilon_{pl} = \mathscr{H}^{-1}(\sigma, \varepsilon_{pl}, v_\gamma)d\sigma \tag{10}$$
$$d\varepsilon_{cr} = \mathscr{A}(\sigma, \varepsilon_{cr}, w_\beta)dt \tag{11}$$
$$dv_\xi = \mathscr{M}_\xi(\sigma, \varepsilon_{pl}, v_\gamma)d\sigma \tag{12}$$
$$dw_\zeta = \mathscr{M}_\zeta(\sigma, \varepsilon_{cr}, w_\beta)d\sigma \tag{13}$$

where each internal variable is either dependent on the plastic strain or the creep strain, but not both. Accordingly, the internal variables are divided into two sets denoted $v_\gamma$ and $w_\beta$, with $\gamma = 1, 2, ..$ and $\beta = 1, 2, ....$ In this way, the plastic strain increment is completely unaffected by the creep strain, and vice versa.

*2.1.3.2. Unified inelastic strain.* For unified inelastic strain, the effect of inelastic strain accumulation is only imposed in terms of a the combined inelastic strain variable $\varepsilon_{pl} + \varepsilon_{cr}$, such that the effect is the same regardless of how inelastic strain is generated, *i.e.* whether it is under creep load conditions or due to an instantaneous stress increase. Hence,

$$d\varepsilon_{pl} = \mathscr{H}^{-1}(\sigma, \varepsilon_{pl} + \varepsilon_{cr}, v_\gamma)d\sigma \tag{14}$$
$$d\varepsilon_{cr} = \mathscr{A}(\sigma, \varepsilon_{pl} + \varepsilon_{cr}, v_\gamma)dt \tag{15}$$
$$dv_\xi = \mathscr{M}_\xi(\varepsilon_{pl} + \varepsilon_{cr}, v_\gamma)d\varepsilon_{in} \tag{16}$$

where $d\varepsilon_{in} = d\varepsilon_{pl} + d\varepsilon_{cr}$. In this way, irrespective of whether inelastic strain is due to a plastic or creep strain increment, the change in all other internal variables will be the same, *e.g.* creep straining causes the same hardening as an equal amount of plastic straining would have done.

## 2.2. Creep strain assessment in SSRT tests

A methodology to assess the creep strain and creep strain rate from isothermal and uniaxial load conditions based on the decoupled and unified inelastic strain partitioning assumptions is now presented.

*2.2.1. Decoupled inealstic strain*

If the stress is applied monotonically, *i.e.* $\dot{\sigma} > 0$ for all $t > 0$, the internal variables $\varepsilon_{pl}$ and $v_\gamma$ in the decoupled formulation must be single-valued function of $\sigma$ (but not necessarily monotonic) through integration of Eqs. 10 and 12, since both differentials are unaffected by time. Hence,

$$d\varepsilon_{pl} = \mathscr{H}^{-1}(\sigma, \varepsilon_{pl}(\sigma), v_\gamma(\sigma))d\sigma = h^{-1}(\sigma)d\sigma \tag{17}$$

where $h$ will be denoted as the hardening modulus, or rate of hardening, *i.e.* the slope of the stress-inelastic strain curve in the case of negligible creep. The expression for the total inelastic strain combining Eqs. 11 and 17 then is

$$d\varepsilon_{in} = h^{-1}(\sigma)d\sigma + \mathscr{A}(\sigma, \varepsilon_{cr}, w_\beta)dt \tag{18}$$

which by rearrangement and integration yields the following expression of the creep strain

$$\varepsilon_{cr}(t) = \int_0^t \mathscr{A}(\sigma, \varepsilon_{cr}, w_\beta)dt = \varepsilon_{in}(t) - \int_0^{\sigma(t)} h^{-1}(\sigma)d\sigma \tag{19}$$

where $\varepsilon_{in}$ is the inelastic strain at any instant $t \geqslant 0$ in a SSRT conducted with an arbitrary load rate $\dot{\sigma} \geqslant 0$.

The creep strain for decoupled inelastic strain partitioning is unaffected regardless of whether the SSRT test is performed in strain or stress control, as long as the stress rate $\dot{\sigma}$ is positive. However, if the test is strain-controlled, as in this investigation, there is a risk of the test material manifesting softening, *i.e.* a negative stress change, for which the premises Eq. 17 is not valid. On the other hand, it is well motivated to assumed that $h^{-1}(\sigma)$ is zero when $\dot{\sigma} < 0$ since otherwise, a negative stress increment at a positive value of stress $\sigma$ would result in a negative plastic strain increment, which is regarded unlikely. Thus, for SSRT tests which manifest softening starting from a maximum stress $\sigma_{max}$ occurring at the time instant $t_{max}$, the creep strain can be assessed as

$$\varepsilon_{cr}(t) = \begin{cases} \varepsilon_{in}(t) - \int_0^{\sigma(t)} h^{-1}(\sigma)d\sigma & t < t_{max} \\ \varepsilon_{in}(t) - \int_0^{\sigma_{max}} h^{-1}(\sigma)d\sigma & t \geqslant t_{max} \end{cases} \tag{20}$$

instead of Eq. 19.

*2.2.2. Unified inelastic strain*

A similar expression for the creep strain by the unified inelastic strain assumption is possible if a restriction is made to materials behaviours involving a yield criterion dictating the rate-independent behaviour. Effectively, it is assumed there is a yield surface $f(\sigma, \varepsilon_{pl} + \varepsilon_{cr}, v_\gamma) \leq 0$, where yielding is represented by $f = 0$, and an associated loading-unloading condition. Notably, despite if $f < 0$, the yield surface may move and expand due to the explicit evolution of the internal variables with time, Eqs. 15 and 16, for the unified inelastic strain behaviour. Thus, the loading-unloading criterion must reflect that unloading occurs if the yield surface evolution with time exceeds the effect of an instantaneous increase in stress, *i.e.* plastic flow occurs if

$$f = 0, \quad \frac{\partial f}{\partial \sigma}d\sigma > \frac{\partial f}{\partial \varepsilon_{in}}\mathscr{A}dt + \frac{\partial f}{\partial v_\xi}\mathscr{M}_\xi\mathscr{A}dt = \frac{\partial f}{\partial t}dt \tag{21}$$

where $\varepsilon_{in} = \varepsilon_{pl} + \varepsilon_{cr}$. Accordingly, the total inelastic strain is written as

$$d\varepsilon_{in} = \begin{cases} \mathscr{H}^{-1}(\sigma, \varepsilon_{pl} + \varepsilon_{cr}, v_\gamma)d\sigma & f = 0, \quad \frac{\partial f}{\partial \sigma}d\sigma > \frac{\partial f}{\partial t}dt \\ \mathscr{A}(\sigma, \varepsilon_{pl} + \varepsilon_{cr}, v_\gamma)dt & \text{otherwise} \end{cases} \tag{22}$$

where $\mathscr{A} = 0$ when yielding, as it is supposed that the yield criteria is associated with time-independent plastic straining only. Thus, we consider unified inelastic strain behaviours for which rate-independence is achieved at high load rates due to the fulfilment of a yielding criterion, whereas rate-dependency occurs at low load rates as soon as the criterion is unfulfilled. This is in agreement with many previously proposed viscoplastic formulations considering unified inelastic strain, *e.g.* [41,51].

As experimentally observed in the present study, the test materials manifest a rate-independent behaviour when loaded at constant strain rate up to a limit stress at which the stress-strain curves deviates from the rate-independent response and become rate-dependent, see Section 4.2. In such cases, rearrangement and integration of Eq. 22 becomes

$$\varepsilon_{cr}(t) = \begin{cases} 0 & t \leqslant t_0 \\ \int_{t_0}^t \mathscr{A}(\sigma, \varepsilon_{pl} + \varepsilon_{cr}, v_\gamma)dt = \varepsilon_{in}(t) - \int_0^{\sigma(t_0)} h^{-1}(\sigma)d\sigma & t > t_0 \end{cases} \tag{23}$$

where $\varepsilon_{in}$ is the inelastic strain at any instant $t \geqslant 0$ in a SSRT test, $t_0$ is the time where the stress-strain curve deviates from the rate-independent stress-strain curve and $h$ is the hardening modulus, *i.e.* the slope of the stress-inelastic strain curve in the case of negligible creep.

*2.2.3. Graphical interpretation of decoupled and unified inelastic strain partitioning*

The assessment of the creep strain when assuming a decoupled inelastic strain, Eq. 20, and a unified inelastic strain, Eq. 23, in a SSRT test can be graphically visualised to ease the understanding, see Fig. 2. For decoupled inelastic strain partitioning, the creep strain at a given instant $t$ can be interpreted as the horizontal distance between the current stress-strain location $(\varepsilon(t), \sigma(t))$ and the rate-independent stress-strain curve observed at high load rates for which the time-dependent effects are negligible. In contrast, the creep strain when assuming a unified inelastic strain partitioning is simply the total inelastic strain determined at the current stress-strain location $(\varepsilon(t), \sigma(t))$ minus the inelastic strain at the instant when the stress-strain curve deviates from the rate-independent stress-strain curve. As a consequence, it should be noted that if the stress-strain curve deviates before the rate-independent yield stress is reached, the creep strain simply becomes the total inelastic strain observed in a SSRT test.

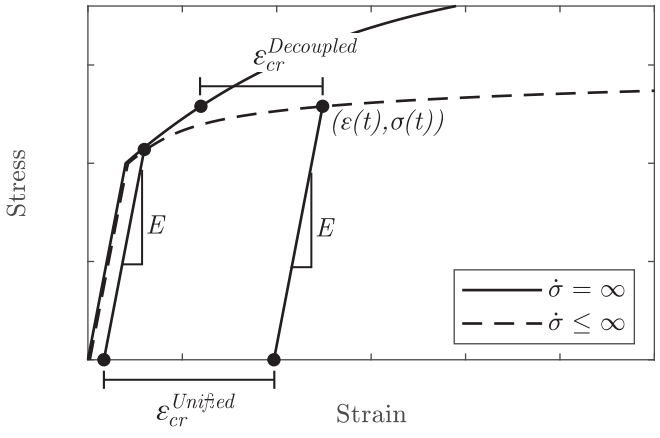


**Fig. 2.** Graphical assessment of the uniaxial creep strain under isothermal tensile test load conditions, based on the decoupled ($\varepsilon_{cr}^{Decoupled}$) and the unified ($\varepsilon_{cr}^{Unified}$) inelastic strain partitioning assumptions. For the former, the creep strain equals the horizontal distance between the current stress-strain location $(\varepsilon(t), \sigma(t))$ and the stress-strain curve when performed in the high load-rate limit, for which the time-dependent effects are negligible, whereas for the latter, the creep strain equals the total inelastic strain at the current stress-strain location $(\varepsilon(t), \sigma(t))$ minus the inelastic strain at the instant when the stress-strain curve deviates from the rate-independent stress-strain curve.

## 3. Materials and experimental procedure

### 3.1. Materials

For the purpose of the present study, a varied set of frequently employed engineering alloys have been investigated, namely, AISI 316L, Hastelloy X and EN-GJS-SiMo5-1. AISI 316L is a solid-solution strengthened austenitic stainless steel typically used in high-temperature applications such as power plants [52,53]. The specimens were taken from a rod that was hot rolled and annealed before cold drawn. The annealing procedure before the cold drawning was performed at 1060 °C during 0.5$h$ and finally quenched in water.

Hastelloy X is a solid-solution strengthened nickel-base superalloy typically used in high-temperature applications, *e.g.* gas turbines [54]. Similarly, the specimens were taken from a rod that was hot rolled and solution annealed, followed by solution annealing at 1175 °C during 0.3$h$ and quenching in water.

Regarding the ductile cast iron EN-GJS-SiMo5-1 commonly used in heavy-vehicle automotive industry [6,15,55], the specimen were extracted from plates, cast with an average cooling rate of 3.5°/C and subjected to a solution treatment at 900°C and a subsequent normalisation in order to generate a fully ferritic matrix. The chemical compositions for the three materials are given in weight percent in Tables 1–3. The elastic modulus and off-set yield strength ($R_{p0.2}$) of each material was determined from the tensile test conducted with $10^{-3}$ $s^{-1}$ strain rate according to standard [56,57], are presented in Table 4.

### 3.2. Mechanical testing

In order to evaluate the creep assessment method presented in Section 2, SSRT tests of the materials presented in Section 3.1, was conducted and validated by conventional creep and stress-relaxation tests. All mechanical tests were performed using an Instron 5982 electromechanical machine and the software Bluehill 3, equipped with an Instron SF16 furnace and an Instron 7361C extensometer with gage length of 12.5 mm. The temperature was kept constant over the whole gauge length by controlling three heating sections in the furnace and the temperature was always allowed to stabilized for two hours before each test. The test temperatures were selected according to the relevant creep temperature regime for each engineering alloy, namely 500 °C for EN-GJS-SiMo5-1, 600 °C for AISI 316L and 800 °C for Hastelloy X. Moreover, the same cylindrical specimen geometry with a 5 mm diameter and a 24.5 mm parallel length was used for all tests, see Fig. 3.

#### 3.2.1. Slow-strain-rate testing (SSRT)

High-temperature tensile tests were performed at strain rates presented in Table 5, one test for each test condition, in crosshead position control, according to the ISO 6892-2 standard [56]. Typically, conventional tensile testing covers strain rates from $10^{-2}$ $s^{-1}$ down to $10^{-4}$ $s^{-1}$, while tensile test at strain rates less than $10^{-3}$ $s^{-1}$ is denoted as slow-strain-rate testing (SSRT) [28,29,58], which was primarily developed for stress corrosion testing, see the ISO 7539-7 standard [59].

#### 3.2.2. Creep tests

To validate the above assessment of creep strain from the SSRT tests, conventional creep tests were performed in load control according to ISO 204 standard [11]. Accordingly, specimens were subjected to a strain rate of $10^{-3}$ $s^{-1}$ in crosshead position control until the pre-defined stress values were reached, see Table 6, at which the tests were immediately switched to load control and a constant stress was maintained until fracture.

#### 3.2.3. Stress-relaxation tests

For further comparisons, stress-relaxation tests in crosshead position control were performed starting from the pre-defined stress values in Table 6, according to ASTM E328 standard [60]. Specimens were initially loaded at a strain rate of $10^{-3}$ $s^{-1}$) until the pre-defined stress values were reached, from which a constant crosshead position was held and the subsequent evolution of the measured stress and strain was recorded.

Following previous investigators [25,61–66], the inelastic strain accumulation during the uniaxial stress relaxation tests $\Delta\varepsilon_{in}$ is typically assessed under the condition

$$\Delta\varepsilon = \frac{\Delta\sigma}{E} + \Delta\varepsilon_{in} = 0 \tag{24}$$

where $E$ is the elastic modulus, $\Delta\varepsilon$ is the strain measured by the extensometer and $\Delta\sigma$ is the uniaxial stress, relative to the strain and stress value, respectively, at the starting time of the hold time. However, rather than a constant value on the extensometer strain $\varepsilon$, the stress change was recorded while subjecting the specimen to a constant crosshead position, hence $\Delta\varepsilon$ was not strictly equal to zero. For this reason, the inelastic strain accumulation was assessed as

$$\Delta\varepsilon_{in} = \frac{\Delta\sigma}{E} - \Delta\varepsilon \tag{25}$$

in the stress-relaxation tests.

#### 3.2.4. SSRT test with an intermediate dwell time

SSRT tests with an intermediate dwell time were performed in order to justify whether any of the two investigated assumptions applies to the tested materials. To this end, specimens were initially loaded with a strain rate of $10^{-3}$ $s^{-1}$ in crosshead position control until the pre-defined stress values were reached, see Table 6. From this instant, the specimens were held at constant load for an increase of approximately 2% in engineering strain. After the dwell time, the specimens were again loaded using a strain rate of $10^{-3}$ $s^{-1}$ in crosshead position control.

### 3.3. Creep strain and creep strain rate assessment by the inelastic strain partitioning

The uniaxial creep strain was assessed from the SSRT tests using Eqs. 20 and 23, as illustrated by the graphical procedure presented in Section 2.2.3. To this end, the SSRT test conducted at the strain rate of $10^{-3}$ $s^{-1}$ mentioned in Table 5 were considered as sufficiently rapid to represent the rate-independent stress-strain curve, which is required to assess the hardening modulus $h$ and the corresponding integral over stress in Eqs. 19 and 23. Accordingly, the inelastic strain $\varepsilon_{in}$ at any instant $t$ in a SSRT test was assessed as

$$\varepsilon_{in}(t) = \varepsilon(t) - E\sigma(t) \tag{26}$$

**Table 1**
Chemical composition of AISI 316L in weight percent. The iron content is implicit.

| C | N | Si | Mn | Cr | Mo | Cu | Ni |
|---|---|---|---|---|---|---|---|
| 0.01 | 0.06 | 0.47 | 1.51 | 16.87 | 2.04 | 0.46 | 10.16 |

**Table 2**
Chemical composition of Hastelloy X in weight percent. The nickel content is implicit.

| C | Si | Mn | Co | Cr | Cu | Fe | Mo | W |
|---|---|---|---|---|---|---|---|---|
| 0.07 | 0.29 | 0.42 | 1.10 | 21.76 | 0.10 | 18.65 | 8.70 | 0.74 |

**Table 3**
Chemical composition of EN-GJS-SiMo5-1 in weight percent. The iron content is implicit.

| C | Si | Mn | S | P | Ni | Mo | Cu | Sn | Ti | Al |
|---|---|---|---|---|---|---|---|---|---|---|
| 3.16 | 4.33 | 0.41 | 0.008 | 0.014 | <0.05 | 0.91 | 0.07 | <0.001 | 0.017 | 0.017 |

**Table 4**
Elastic moduli and 0.2% off-set yield strength ($R_{p0.2}$) at elevated temperatures for EN-GJS-SiMo5-1, AISI 316L and Hastelloy X.

| Material | Temperature [°C] | Elastic modulus [GPa] | Yield strength [MPa] |
|---|---|---|---|
| EN-GJS-SiMo5-1 | 500 | 148.3 | 337.7 |
| AISI 316L | 600 | 175.5 | 380.2 |
| Hastelloy X | 800 | 136.7 | 239.4 |

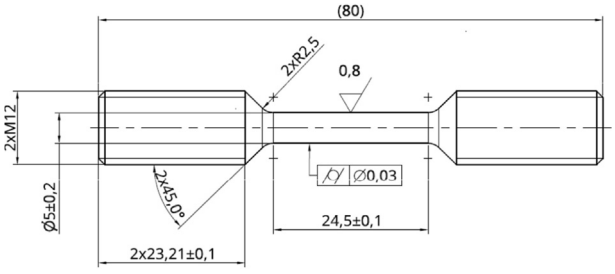


**Fig. 3.** Drawing of the cylindrical specimen geometry used for all mechanical tests.

**Table 5**
Strain rates used for the SSRT tests of EN-GJS-SiMo5-1, AISI 316L and Hastelloy X. One specimen was tested for each test condition.

| Material | Strain rates [$s^{-1}$] |
|---|---|
| EN-GJS-SiMo5-1 | $10^{-3}$ $s^{-1}$, $10^{-5}$ $s^{-1}$, $10^{-6}$ $s^{-1}$ |
| AISI 316L | $10^{-3}$ $s^{-1}$, $10^{-5}$ $s^{-1}$, $10^{-6}$ $s^{-1}$ |
| Hastelloy X | $10^{-2}$ $s^{-1}$, $10^{-3}$ $s^{-1}$, $10^{-4}$ $s^{-1}$, $10^{-5}$ $s^{-1}$, $10^{-6}$ $s^{-1}$ |

**Table 6**
Pre-defined stress levels for the creep, stress-relaxation and SSRT-dwell tests. One specimen was tested for each test condition.

| *Material* | *Creep stresses* [MPa] | *Relaxation stresses* [MPa] | *Dwell stresses* [MPa] |
|---|---|---|---|
| EN-GJS-SiMo5-1 | 200, 250, 300 | 355 | 280 |
| AISI 316L | 380, 400, 450 | 440 | 380 |
| Hastelloy X | 110, 170, 230 | 300 | 200 |

where $\varepsilon$ is the engineering strain recorded by the extensometer, $\sigma$ is the engineering stress, *i.e.* the applied force divided by the initial cross-sectional area of the specimen, and $E$ is the elastic modulus measured in the SSRT test performed with $10^{-3}$ $s^{-1}$, see Table 4. The creep strain was in turn acquired by subtracting the inelastic strain data acquired at the high strain rate of $10^{-3}$ $s^{-1}$ with those acquired at slow strain rates, $10^{-5}$ $s^{-1}$ and $10^{-6}$ $s^{-1}$, according to the developed methodology for decoupled and unified inelastic strain illustrated in Fig. 2.2.3.

Since the subtraction of inelastic strain data involves inelastic strain measured in two separate test specimens, the accuracy at low creep strain values is considered low due to the possible variation between test specimens even though the material is nominally the same. However, at large creep strain values, the eventual error is negligible compared to the measured creep strain, hence the error is only significant at small creep values. For this reason, creep strain values below 0.05% was consistently disregarded and not included in the creep assessment by this method.

Furthermore, the AISI 316L material manifested dynamic strain ageing for the tested temperature when subjected to the strain rate of $10^{-3}$ $s^{-1}$, see Fig. 4b. To avoid interference with the creep strain assessment, the strain bursts were removed by removing all stress-strain points lying more than 1 MPa off the smoothed stress-strain curve obtained using a moving average with a fixed window length of 0.25% strain.

To assess the creep strain rate, the acquired creep strain was differentiated with respect of time using the incremental polynomial method with a fitting set size of 201 successive data points, as for instance described in the E647 standard [67].

## 4. Results and discussion

The purpose of the performed mechanical testing described in the previous section is to evaluate the validity of the proposed accelerated creep assessment method based on inelastic strain partitioning assumptions presented in Section 2. To this end, the partitioning assumptions, namely the decoupled and unified inelastic strain, and the creep assessment method are separately investigated. It is important to note that the variation in mechanical behaviour observed in Section 4.1 is not only due to the variation in materials, but is also a result of testing at different temperatures, which were individually selected for each alloy to lie in the temperature range where creep is active [53,54].

### 4.1. Mechanical behaviour at high temperatures

The mechanical data of relevance for this study acquired from tensile, creep and stress relaxation tests described in Section 3.2 are shown in Figs. 4–7, namely high-temperature engineering stress-strain, creep and stress relaxation curves. The engineering stress-strain curves for EN-GJS-SiMo5-1 at all strain rates in Fig. 4a manifest a flat appearance after the initial yield stress, which indicates that no significant work hardening is occurring at the tested temperature. However, in Fig. 4a EN-GJS-SiMo5-1 shows softening when deformed using a strain rate of $10^{-6}$ $s^{-1}$. On the contrary, both AISI 316L and Hastelloy X show an increasing curve after the initial yield stress at high strain rates, hence these materials appears to harden with increasing deformation as long as the load rate is sufficiently high. This is visible in Fig. 4b for AISI 316L at the strain rate of $10^{-3}$ $s^{-1}$ and in Fig. 4c for Hastelloy X at the strain rates of $10^{-2}$–$10^{-4}$ $s^{-1}$. However, with decreasing strain

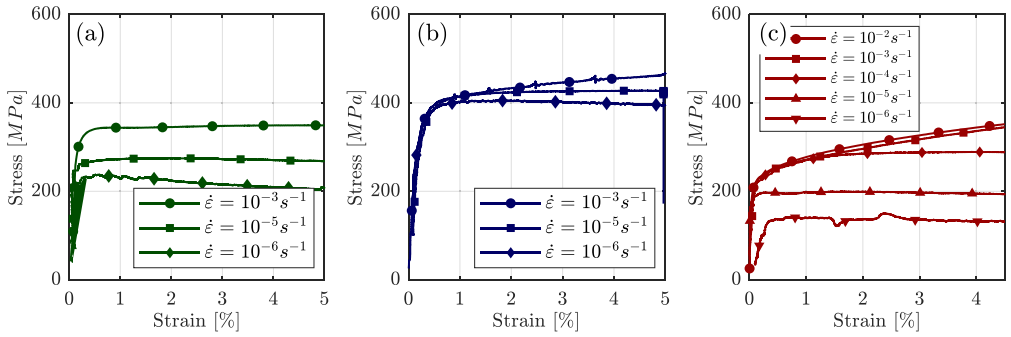


**Fig. 4.** Stress-strain curves of high-temperature tensile tests performed with different strain rates at temperatures of 500, 600 and 800 °C for (a) EN-GJS-SiMo5-1, (b) AISI 316L and (c) Hastelloy X respectively.

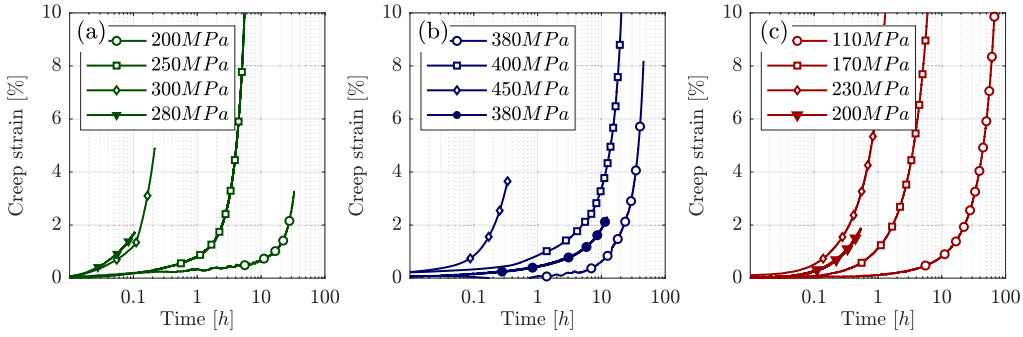


**Fig. 5.** Evolution of creep strain in uniaxial creep tests performed with different constant stress levels at temperatures of 500, 600 and 800 °C for (a) EN-GJS-SiMo5-1, (b) AISI 316L and (c) Hastelloy X respectively. The creep strain accumulated during the constant-stress period in the SSRT with an intermediate dwell time are included and displayed with solid markers.

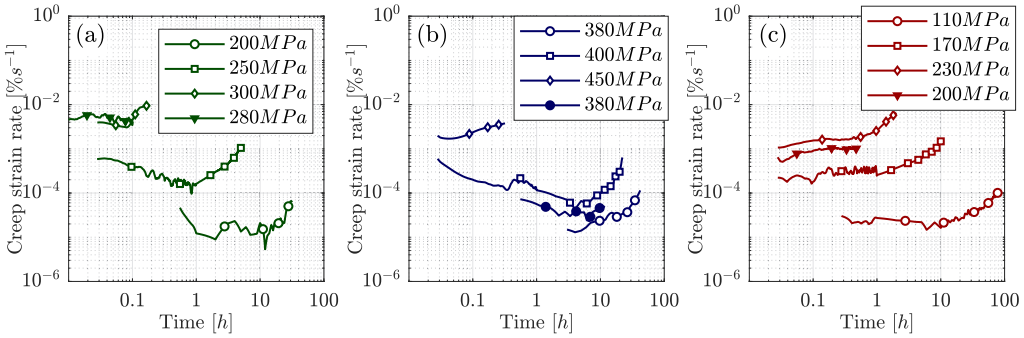


**Fig. 6.** The creep strain rate in uniaxial creep tests performed with different constant stress levels at temperatures of 500, 600 and 800 °C for (a) EN-GJS-SiMo5-1, (b) AISI 316L and (c) Hastelloy X respectively. The creep strain rate evaluated during the constant-stress period in the SSRT with an intermediate dwell time are included and displayed with solid markers.

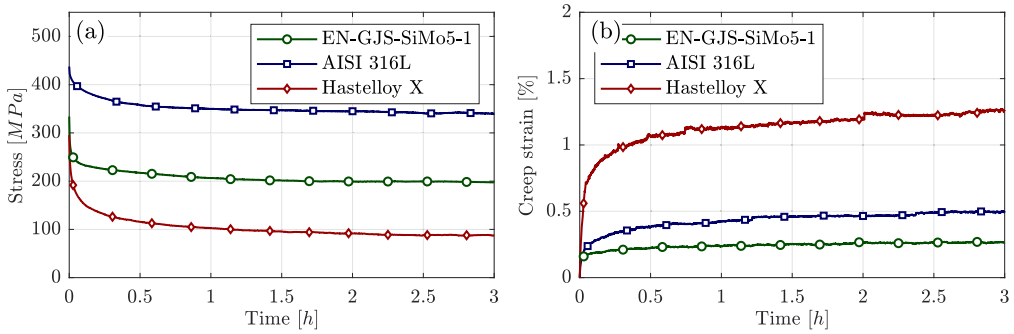


**Fig. 7.** The (a) measured uniaxial stress as a function of time and (b) the corresponding creep strain estimated by Eq. 25, in stress-relaxation tests starting stress of 355, 440 and 300 MPa and at temperatures of 500, 600 and 800 °C for EN-GJS-SiMo5-1, AISI 316L and (c) Hastelloy X respectively.

rate, the mechanical behaviour changes. When using strain rates below $10^{-5}$ $s^{-1}$, the work hardening in AISI 316L and Hastelloy X decreases to become a flat curve as similar to the mechanical behaviour of EN-GJS-SiMo5-1. Notably, the initial yield stress decreases with decreasing strain rate, which can be observed for all tested alloys in Fig. 4, compare for example the yield stresses of EN-GJS-SiMo5-1 when subjected to strain rates of $10^{-3}$ $s^{-1}$, $10^{-5}$ $s^{-1}$ and $10^{-6}$ $s^{-1}$ in Fig. 4a. Regarding the high yield stress of AISI 316L in the current study compared to AISI 316L studied elsewhere [68], it is much likely due to the cold worked condition. In addition, it is further noted in Fig. 4b, that striations appear in AISI 316L when yielding at the strain rate of $10^{-3}$ $s^{-1}$, which is interpreted as dynamic strain ageing (DSA) [58,68]. DSA originates from interaction between solute atoms and dislocations during plastic deformation. Under plastic flow, dislocations are gliding until they come across an obstacle where they are stationary until the obstacles are surmounted. When the dislocations are stationary, solute atoms can diffuse towards the dislocations which results in an increase in the activation energy for further slip and consequently also an increase in the stress needed for overcoming the obstacle [69].

In Fig. 5, the creep strain as a function of time at constant applied stress is presented for the three alloys. As seen in the figure, the selected stress levels impose relatively short durations of the tests, however they were selected with the purpose of being the same range as the stress levels attained in the SSRT tests. Moreover, the primary, secondary and tertiary creep stages are not easily identified in Fig. 5 due to the logarithmic axis. Instead, the creep stages can be identified in Fig. 6, where the creep strain rate over time is presented for each alloy. Fig. 6 shows a high creep strain rate in the beginning, *i.e.* primary creep stage, for some of the tested alloys and test conditions, namely for EN-GJS-SiMo5-1 tested at 200 MPa and 250 MPa and for AISI 316L tested at 400 MPa. For Hastelloy X and the other test conditions no primary creep stage was observed. The minimum creep strain rate in Fig. 6, *i.e.* the secondary creep stage, is present for all tested alloys and conditions and the same is valid for the tertiary creep stage corresponding to the increases in the creep rate after the minimum creep strain rate in Fig. 6.

From the stress relaxation curves in Fig. 7, it is observed that the stress relaxation and consequently the increase in calculated creep strain are the highest in the beginning of the test followed by a decrease in the changes of stress relaxation and creep strain.

### 4.2. Evaluation of the validity of inelastic strain partitioning assumptions

Before evaluating the creep assessment presented in Section 2.2, the validity of inelastic strain partitioning assumptions must be investigated. Firstly, as postulated in Section 2.1.2, an infinitesimal increase in inelastic strain at any instant may have two contributions, a creep increment due to passage of time and a plastic increment caused by an increase in stress, see Eq. 6. Thus, it is imposed that the plastic strain component must characterise the stress-strain curve at high load rates for which there is not enough time to cause accumulation of creep strain, see Eq. 9. Consequently, performing SSRT tests with increasing load rate should indicate a convergence to a unique rate-independent stress-strain curve, as is observed for Hastelloy X and ASIS 316L, see Figs. 4b and 4c. Notably, convergence is first attained at low stresses, *e.g.* see $\dot{\varepsilon} = 10^{-5}$ and $\dot{\varepsilon} = 10^{-6}$ in Fig. 4c, whereas overlap at higher stresses requires increasingly higher load rates, see $\dot{\varepsilon} = 10^{-3}$ and $\dot{\varepsilon} = 10^{-4}$ in Fig. 4c. This behaviour is simply interpreted as the rate of accumulation of creep strain being more significant at higher stresses, which hence requires higher load rate in order to be suppressed.

Regarding the inelastic strain partitioning assumptions, their validity can be explicitly tested by performing SSRT tests with intermediate dwell time in comparison to SSRT without interruptions, as discussed in Section 2.1.3. As the assumptions are formulated, the subsequent tensile loading following an intermediate constant-stress dwell time will either result in an elastic load path attaining the no-dwell curve or an unaffected continuation of the hardening curve, see Fig. 1, if either the unified or decoupled partitioning assumption, respectively, is applicable. Effectively, Fig. 8 shows the stress-strain curve of the tested materials when subjected to a strain rate of $10^{-3}$ $s^{-1}$ and an intermediate dwell time of approximately 2% engineering creep strain, compared to a SSRT test with the same strain rate but without dwell.

In order to make the illustration of the effect of the dwell time on subsequent hardening even better, the same comparison is shown in Fig. 9, however, with the stress-strain curves of the load segment ensuing the dwell time horizontally translated such that the end of the dwell time coincides with the stress-strain curve without dwell. In this way, it is made clear that EN-GJS-SiMo5-1 and Hastelloy X manifest a similar behaviour for which the dwell time imposes an apparent increase in the flow stress, see Figs. 9a and c. The increase in flow stress is significant for Hastelloy X, roughly in the range of 50–80 MPa, see Fig. 9c, whereas for EN-GJS-SiMo5-1 it is much less, 10–30 MPa, see Fig. 9a. Accordingly, it is noted that the difference in the increase in flow stress between the two materials is much related to behaviour demonstrated in Fig. 8a and c, *i.e.* that the tensile loading ensuing the dwell time tends to bring back the stress to the stress-strain curve without dwell. Thus, since the hardening rate, *i.e.* the slope of the stress-strain curve during inelastic deformation, is much higher in Hastelloy X compared to EN-GJS-SiMo5-1, a much higher stress increase is required to come back to the stress-strain curve without dwell in Hastelloy X. In contrast for EN-GJS-SiMo5-1, the hardening rate approaches zero as the strain increases. Hence, even though the flow stress is increased by the dwell time, the two curves still coincide as the saturated flow stress is reached, see 8a.

As opposite to EN-GJS-SiMo5-1 and Hastelloy X, AISI 316L manifests a behaviour for which the dwell time does not influence the flow stress remarkably, see Fig. 9b. However, looking more closely, there is a small stress increase at the instant of load application in the end of the dwell time, see Fig. 9b. The stress peak is intepreted as DSA, where solute atoms can diffuse towards the dislocations which result in an increase in stress needed for overcoming the obstacle [69]. In addition, DSA is present in the curve without dwell time and have been reported occuring in AISI 316L within the used strain rate and temerature [58,68]. Nevertheless, the effect is small, and the flow stress is not much different from the tensile test without dwell.

When at larger strain values in AISI 316L, $> 0.5\%$, the curves deviate in Fig. 9b, where the tensile test subjected to an intermediate dwell is situated below the tensile test without dwell. Thus, it is indicated that the dwell time has reduced the hardening rate of the subsequent tensile loading. On the other hand, it must be emphasised that the two tests, *i.e.* the tensile test with and without intermediate dwell, are performed on two different test specimens. Hence, a difference may also arise due to the variations between specimens, which in fact, is a likely explanation for the hardening difference observed in AISI 316L. Looking more closely at the stress-strain curves, see Fig. 10, there is roughly a 10 MPa difference before the dwell time despite the same strain rate, which corresponds well to the stress difference seen in Fig. 9b. For this reason, the deviation seen in Fig. 9b is considered to be due to variations between test specimens, rather than an effect of the dwell time on the hardening behaviour. Similarly, the two curves of Hastelloy X do not perfectly coincide at large strains either, however here, the dwell time seems to increase the subsequent

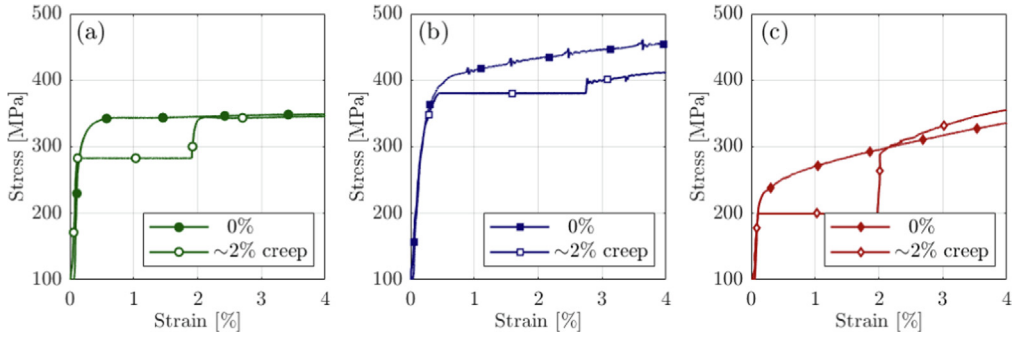


**Fig. 8.** Tensile test curves of (a) EN-GJS-SiMo5-1 at 500 °C, (b) AISI 316L at 600 °C and (c) Hastelloy X at 800 °C when subjected to a strain rate of $10^{-3}$ $s^{-1}$ with and without an intermediated dwell time corresponding to approximately 2% engineering creep strain.

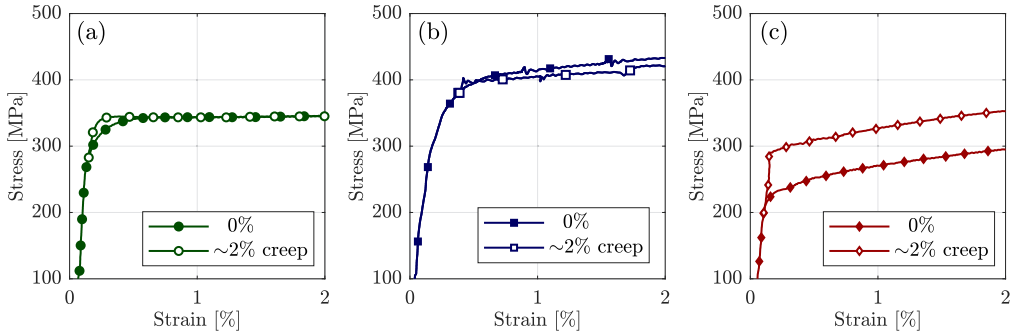


**Fig. 9.** Tensile test curves of (a) EN-GJS-SiMo5-1 at 500 °C, (b) AISI 316L at 600 °C and (c) Hastelloy X at 800 °C when subjected to a strain rate of $10^{-3}$ $s^{-1}$ with and without an intermediated dwell time corresponding to approximately 2% engineering creep strain. In contrast to Fig. 8, the stress-strain curves of the load segment ensuing the dwell time are horizontally translated such that the end of the dwell time coincides with the stress-strain curve without dwell, in order to highlight the effect on the flow stress.

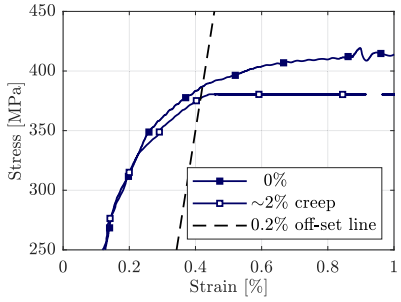


**Fig. 10.** A closer view of Fig. 8b to illustrate the difference between test specimens. Even though the specimen are of the same material, AISI 316L, and subjected to the same initial strain rate of $10^{-3}s^{-1}$, the flow stress differs. An off-set line with a slope equal to the elastic modulus illustrates a difference in the off-set yield strength value of roughly 10 MPa between the specimens.

hardening rate rather than decreasing it. In this case, there is unfortunately no possibility to distinguish whether it is due to an influence of the dwell time or simply a result of testing two different specimens.

Despite the limitations in comparing tensile tests with and without intermediate dwell, the above analysis still provides a rough idea whether the ideal decoupled and unified behaviour put forth in Section 2.1.3 are reasonable by comparison to Fig. 1. As seen in Figs. 8a and c, EN-GJS-SiMo5-1 and Hastelloy X clearly manifest a unified inelastic strain behaviour motivated by the observation that the creep strain accumulated during an intermediate dwell time results in a flow stress increase comparable to the increase in flow stress caused by the inelastic straining though high strain-rate tensile loading. In contrast, AISI 316L manifests a distinct decoupled inelastic strain behaviour as the effect of the intermediate dwell does not affect the flow stress, see Fig. 9b, as opposite to the two former alloys. Thus, by these experiments, it is justified to assume that AISI 316L comply to a decoupled inelastic strain behaviour whereas the unified inelastic strain assumption is applicable for EN-GJS-SiMo5-1 and Hastelloy X.

Different mechanistic reasons to why different materials comply to different inelastic strain partitioning principles can be discussed. However, this study do not aim to examine them in detail rather to address them for future work. Differences in crystal structures, deformation mechanisms, phase stability and recovery mechanisms between the tested materials or a complex combination of these aspects may possibly relate to the inelastic strain partitioning behaviour. Regarding the crystal structures the ferritic EN-GJS-SiMo5-1 and the austenitic AISI 316L and Hastelloy X have a body-centred-cubic and a face-centred-cubic structure respectively. However, this difference cannot be explicitly correlated to different inelastic strain partitioning principles, as both EN-GJS-SiMo5-1 and Hastelloy X behave according to the unified assumption despite different crystal structures. Regarding deformation mechanisms, EN-GJS-SiMo5-1, Hastelloy X and AISI 316L all have similar deformation behaviour consisting of dislocation slip under high-temperature tensile test conditions [37,68,70]. Under creep test conditions, Hastelloy X and AISI 316L manifest dislocation creep [71,72], while it is argued that EN-GJS-SiMo5-1 manifests similar matrix deformation under both tensile and creep load conditions [14]. Hence, there is no clear indication that the underlying deformation mechanisms may account for the observed differences in inelastic strain partitioning. On the other hand, the stability of phases appears to differs between the tested alloys, which can effect the partitioning behaviour if the phase content is changing during the extent of the performed tests. Indeed, all the tested materials are expected to form secondary phases at elevated

temperature [14,55,73,74]. However, it is considered unlikely that the phase stability at high temperatures has a significant influence on the inelastic strain partitioning behaviour, since the time at elevated temperature is relatively short for considerable precipitation. A final possible explanation is differences in recovery mechanisms, as AISI 316L has been reported to show recovery mechanisms such as dynamic recovery and dynamic recrystallisation at the tested temperature [68], whereas EN-GJS-SiMo5-1 and Hastelloy X are less prone to manifest recovery mechanisms at the tested temperatures [75,76]. Thus, recovery is likely to occur in AISI 316L under the tested conditions, especially since it is cold worked, and it is therefore argued to be the most likely cause to why AISI 316L has a decoupled inelastic strain behaviour in contrast to EN-GJS-SiMo5-1 and Hastelloy X.

The association of a decoupled inelastic strain behaviour with materials manifesting recovery can be further motivated. Starting with identifying a flow stress $\sigma_y$ associated with the plastic strain increment $d\varepsilon_p$ as an internal variable, the decoupled inelastic strain assumption implies that the unixial stress $\sigma$ must equal the flow stress $\sigma_y$ at any instant during a monotonic tensile test, $\dot{\sigma} \geqslant 0$, *i.e.*

$$d\sigma_y = d\sigma \tag{27}$$

Combining the above equation with the decoupled inelastic strain partitioning assumption, Eq. 18, the change in the flow stress $d\sigma_y$ is related to inelastic strain and time differentials as

$$d\sigma_y = h d\varepsilon_{in} - h\mathscr{A} dt \tag{28}$$

which in principle is the same expression as the Bailey-Orowan equation [77,78]. In accordance with the original interpretation, $h$ is the rate of strain hardening whereas $h\mathscr{A}$ is the rate of recovery, *i.e.* the decrease in flow stress with time.

### 4.3. Evaluation of the creep assessment method by comparison to stress-relaxation and creep tests

When comparing different creep assessment methods for which different load conditions are involved, it is not straight forward how to make the comparison because the measured creep strain rate is not only dependent on the applied load variables, but typically also evolve with time, see for instance Fig. 6. On the other hand, the creep strain rate is usually seen to be significantly influenced by stress and temperatures, which is the reason for making the comparison in terms of these variables. Effectively, Fig. 11 compares the creep strain rate as a function of stress measured in standard creep tests and assessed from SSRT based on the inelastic strain partitioning method for the three tested materials. In view of the results presented in the previous section, creep strain rate of EN-GJS-SiMo5-1 and Hastelloy X are assessed based on the unified inelastic strain assumption, and AISI 316L based on the decoupled inelastic strain assumption. Again, the creep strain rate in creep tests is generally not constant, *e.g.* see Fig. 6, which is the reason why these data points are vertically elongated in the figure, where each line corresponds to an individual creep test. Similarly, the SSRT data points are also vertically distributed depending on the assessed creep strain rate, as well as horizontally distributed depending on the stress variation during the test, see Fig. 4. Nonetheless, it is observed that the creep strain rate assessed in SSRT lies within the trend band traced out by the creep strain rate data acquired in conventional creep testing, marked out by a pair of solid lines in Fig. 11. Thus, the inelastic strain partitioning method appears to provide creep strain rates in agreement with conventional creep testing.

It must be emphasised that the width of the trend band traced out by the conventionally measured creep rates originates from the variation in creep strain rate over the primary, secondary and tertiary creep stages, which is visualised in Fig. 6. Accordingly, the lower edge of the trend band corresponds to the minimum creep strain rate in the secondary stage whereas the upper edge corresponds to the maximum creep strain which occurs either in the primary or tertiary stage as seen Fig. 6. In contrast, for the creep strain assessed from SSRT data, the distinction of creep stages is less evident. The reason for this is the fact that the stress is not constant in the SSRT tests, hence depending on how the stress varies, the creep strain rate supposedly changes accordingly.

The above point is illustrated in Fig. 12 which shows the creep strain assessed trough inelastic strain partitioning of SSRT tests performed with a strain rate of $10^{-6}$ s$^{-1}$ compared to the creep strain of the conventional uniaxial creep tests. The applied stress in the tests are reported in the figure legends, which in the case of the SSRT tests becomes an interval rather than a constant value. In this way, it is observed that there is hardly any appearance of a primary creep stage in contrast to the conventionally measured creep strain, see for instance AISI 316L in Fig. 12b. Similarly, the creep strain assessed from the SSRT tests of Hastelloy X seems to have a smaller creep rate at the start, see Fig. 12c, which is the opposite compared to the conventional creep tests where the initial creep rate is higher, see Fig. 6c. The reason for this is presumably related to the variable stress of the SSRT tests for which the first onset of creep strain is expected to occur while the applied stress is increasing. In other words, the decrease in creep strain rate normally occurring during the primary creep stage is presumably evened out by the concurrent increase in applied stress in the SSRT test.

A similar remark can be done regarding the tertiary creep stage, which is not as distinct as in the SSRT tests compared to the conventional creep tests, see for instance EN-GJS-SiMo5-1 in Fig. 12a

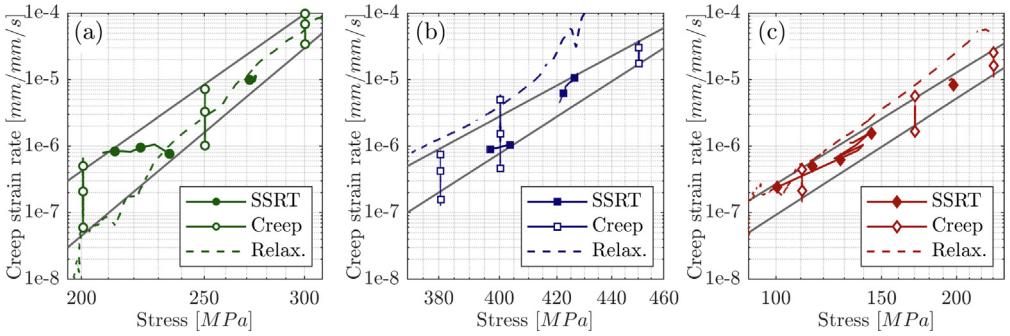


**Fig. 11.** Creep strain rate as a function of stress measured in standard creep tests, see Section 3.2.2, stress-relaxation tests, see Section 3.2.3, and assessed from SSRT test using inelastic strain partitioning, see Sections 3.2.1, for (a) EN-GJS-SiMo5-1 at 500 °C, (b) AISI 316L at 600 °C and (c) Hastelloy X at 800 °C. As motivated by the results presented in Section 4.2, the unified inelastic strain partitioning assumption is employed for EN-GJS-SiMo5-1 and Hastelloy X, whereas the decoupled assumption is used for AISI 316L in the creep strain rate assessment of the SSRT tests.

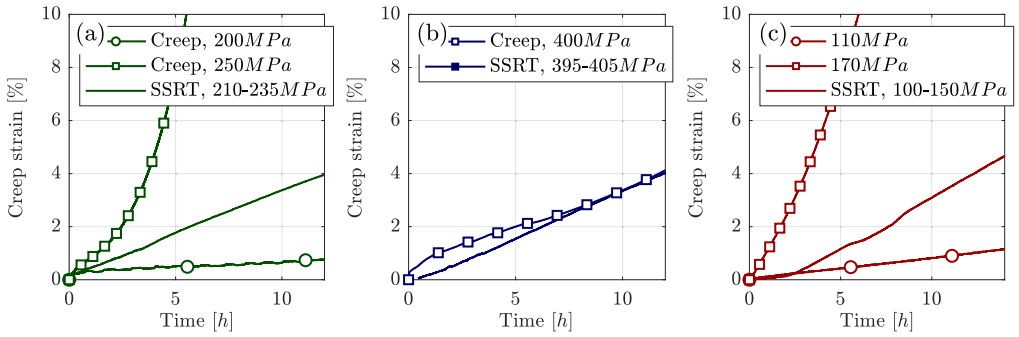


**Fig. 12.** Creep strain evolution with time measured in standard creep tests, see Section 3.2.2, and assessed from SSRT test performed with a strain rate of $10^{-6}s^{-1}$ using inelastic strain partitioning, see Section 3.3, for (a) EN-GJS-SiMo5-1 at 500 °C, (b) AISI 316L at 600 °C and (c) Hastelloy X at 800 °C. As previously, the unified inelastic strain partitioning assumption is employed for EN-GJS-SiMo5-1 and Hastelloy X, whereas the decoupled assumption is used for AISI 316L.

where the creep strain rate appears to decrease rather than increase as opposite to the standard creep test at 250 MPa. On the other hand, the phenomena is well explained by the decreasing stress at high strain values observed in the SSRT test of the EN-GJS-SiMo5-1, see the $10^{-6}$ $s^{-1}$ curve in Fig. 4a, which arguably neutralise the increase in creep strain rate associated with the tertiary creep stage.

Fig. 11 also contains creep strain rates assessed from stress relaxation tests, acquired as explained in Section 3.2.3. It is observed that similar values are acquired in this way compared to conventional creep tests, as well as the SSRT tests through the inelastic strain partitioning method. However, in contrast to the SSRT tests, the creep strain rates assessed by stress relaxation sometimes fall outside the trend band traced out by the conventionally measured creep strain rates, see Figs. 11b and c. Thus, considering the creep strain rates measured in conventional creep tests as the reference, SSRT testing using inelastic strain partitioning appears to provide slightly higher accuracy in the assessment of the creep strain rate compared to stress-relaxation tests.

As related to the discussion connected to Fig. 10 regarding the possible variation between specimens of the nominally same material, it is worth emphasising that only one test per test condition is made and it is reasonable to expect some variations in the assessed creep strain if multiple specimens are tested. Notably, there is evidently some variations when comparing the conventional creep tests with the creep strain accumulation observed in the SSRT tests with intermediate dwell, which up to the end of the dwell time can be considered a creep test, see Figs. 5 and 6. On the other hand, even though there is signs of considerable scatter, its effect is not considered significant because of the consistent trend between the conventional creep and SSRT tests in Fig. 11, which involves multiple tests but at different test conditions. Besides, it is only the scatter in the rate-independent responses which is of concern for the accuracy of the method, in view of the how the creep strain is assessed from SSRT tests, see Fig. 2. Effectively, this variation appears to be considerably smaller compared to the conventional creep tests, see Figs. 4 and 10, and is also accounted for in the assessment by disregarding small creep strains, as described in Section 3.3.

## 5. Conclusions

- It is demonstrated that the inelastic strain in all tested materials when subjected to uniaxial load conditions at elevated temperature can be decomposed into plastic and creep strain component by one of two general inelastic strain partitioning principles. Either, the plastic and creep strain component are non-interacting and additive, as observed in the case of the tested stainless steel AISI 316L at 600°C, referred to as decoupled inelastic strain. Or, as in the case of the ductile cast iron EN-GJS-SiMo5-1 at 500 °C and the nickel-base superalloy Hastelloy X at 800 °C, the plastic and creep strain components are unified, meaning that the effect of an increase in inelastic strain is the same irrespective of whether it is caused through creep at constant stress or by plastic deformation due to an instantaneous stress increase.
- Using conventional uniaxial creep tests as a reference, it is found that the creep strain rate can be accurately assessed from slow-strain-rate testing series using a proposed methodology based on inelastic strain partitioning, assuming either a decoupled or unified inelastic strain. In particular, the new creep assessment method is shown to have better agreement than conventional stress-relaxation tests commoly used to assess the creep performance of materials.

## Data availability

The raw/processed data required to reproduce these findings cannot be shared at this time as the data also forms part of an ongoing study.

## Declaration of Competing Interest

The authors declare that they have no known competing financial interests or personal relationships that could have appeared to influence the work reported in this paper.

## Acknowledgement

The present study was financed by the Swedish Governmental Agency for Innovation Systems (2018-04302), and the Sandvik Materials Technology. Special thanks are also addressed to Peter Skoglund for supplying the SiMo51 materials, Per Johansson for specimen manufacturing and Patrik Härnman for his technical support on the mechanical test machine.

## References

[1] F.A. Leckie, D.R. Hayhurst, Creep Rupture of Structures, Proc. Roy. Soc. A: Math. Phys. Eng. Sci. 340 (1622) (1974) 323–347.
[2] I. Salam, A. Tauqir, A.Q. Khan, Creep-fatigue failure of an aero engine turbine blades, Eng. Fail. Anal. 9 (3) (2002) 335–347.
[3] M.E. Kassner, T.A. Hayes, Creep cavitation in metals, Int. J. Plast. 19 (10) (2003) 1715–1748.
[4] M. Basirat, T. Shrestha, G.P. Potirniche, I. Charit, K. Rink, A study of the creep behavior of modified 9Cr-1Mo steel using continuum-damage modeling, Int. J. Plast. 37 (2012) 95–107.

[5] J.J. Thomas, L. Verger, A. Bignonnet, E. Charkaluk, Thermomechanical design in the automotive industry, Fatigue Fract. Eng. Mater. Struct. 27 (10) (2004) 887–895.
[6] D. Pierce, A. Haynes, J. Hughes, R. Graves, P. Maziasz, G. Muralidharan, A. Shyam, B. Wang, R. England, C. Daniel, High Temperature Materials for Heavy Duty Diesel Engines: Historical and Future Trends, Prog. Mater. Sci. 103 (January 2018) (2018) 109–179.
[7] R.S. Corran, S.J. Williams, Lifing methods and safety criteria in aero gas turbines, Eng. Fail. Anal. 14 (3) (2007) 518–528.
[8] M.A. Ghafir, Y.G. Li, R. Singh, K. Huang, X. Feng, Impact of operating conditions and design parameters on gas turbine hot section creep life, Proc. ASME Turbo Expo 3 (2010) 547–558.
[9] F. Abe, Progress in Creep-Resistant Steels for High Efficiency Coal-Fired Power Plants, J. Pressure Vessel Technol. Trans. ASME 138 (4) (2016) 1–21.
[10] M. Hughes, Challenges for Gas Turbine Engine Components in Power Generation, Procedia Struct. Integr. 7 (2017) 33–35.
[11] ISO, Metallic materials - Uniaxial creep testing in tension - Method of test, 2009.
[12] T. Matsuo, K. Nakajima, Y. Terada, M. Kikuchi, High temperature creep resistance of austenitic heat-resisting steels, Mater. Sci. Eng. 146 (1–2) (1991) 261–272.
[13] Y. Yamamoto, M.P. Brady, Z.P. Lu, P.J. Maziasz, C.T. Liu, B.A. Pint, E.A. Payzant, Creep-resistant, Al2O3-forming austenitic stainless steels, Science 316 (5823) (2007) 433–436.
[14] E. Hug, C. Keller, J. Favergeon, K. Dawi, Application of the Monkman-Grant law to the creep fracture of nodular cast irons with various matrix compositions and structures, Mater. Sci. Eng., A 518 (1–2) (2009) 65–75.
[15] C. Öberg, R. Rablbauer, B. Zhu, S. Jonsson, Monotonic and Cyclic Creep of Cast Materials for Exhaust Manifolds, SAE Int. J. Mater. Manuf. 12 (2) (2019) 5–12.
[16] F. Tancret, T. Sourmail, M.A. Yescas, R.W. Evans, C. McAleese, L. Singh, T. Smeeton, H.K. Bhadeshia, Design of a creep resistant nickel base superalloy for power plant applications: Part 3 - Experimental results, Mater. Sci. Technol. 19 (3) (2003) 296–302.
[17] F. Tancret, M. Bellini, Properties, processability and weldability of a novel affordable creep resistant nickel base superalloy, Mater. Sci. Technol. 24 (4) (2008) 479–487.
[18] O.M. Horst, D. Adler, P. Git, H. Wang, J. Streitberger, M. Holtkamp, N. Jöns, R.F. Singer, C. Körner, G. Eggeler, Exploring the fundamentals of Ni-based superalloy single crystal (SX) alloy design: Chemical composition vs. microstructure, Mater. Des. 195(January 2019) (2020).
[19] N. Mo, Q. Tan, M. Bermingham, Y. Huang, H. Dieringa, N. Hort, M.X. Zhang, Current development of creep-resistant magnesium cast alloys: A review, Mater. Des. 155 (2018) 422–442.
[20] F.R. Larson, A time-temperature relationship for rupture and creep stresses, Trans. Am. Soc. Met. (1952) 765–775.
[21] S.S. Manson, A.M. Haferd, A linear time-temperature relation for extrapolation of creep and stress-rupture data, Tech. rep. (1953).
[22] R.W. Evans, Statistical scatter and variability of creep property estimates in θprojection method, Mater. Sci. Technol. 5 (7) (1989) 699–707.
[23] R.W. Evans, The θprojection method and low creep ductility materials, Mater. Sci. Technol. 16 (1) (2000) 6–8.
[24] D.A. Woodford, Test methods for accelerated development, design and life assessment of high-temperature materials, Mater. Des. 14 (4) (1993) 231–242.
[25] J.Q. Guo, F. Li, X.T. Zheng, H.C. Shi, W.Z. Meng, An Accelerated Method for Creep Prediction From Short Term Stress Relaxation Tests, J. Pressure Vessel Technol. 138 (3) (2016) 0314011–0314015.
[26] U. Kocks, Laws for Work-Hardening and Low-Temperature Creep, J. Eng. Mater. Technol. 98 (1) (1976) 76–85.
[27] D.C. Stouffer, L. Papernik, H.L. Bernstein, An Experimental Evaluation of the Mechanical Response Characteristics of Rene 95, AFWAL-TR-80-4136, Tech. rep., Materials laboratory, University of Cincinnati, Cincinnati, Ohio (1980).
[28] H.-K. Oh, Determination of rupture time and strain rate in creep by means of the uniaxial tensile test, J. Mater. Process. Technol. 59 (4) (1996) 294–296.
[29] Y. Xuexing, R. Sandstrom, Study of creep behaviour in P-doped copper with slow strain rate tensile tests, Tech. rep. (2000).
[30] S. Lee, W.G. Knauss, Note on the determination of relaxation and creep data from ramp tests, Mech. Time-Dependent Mater. 4 (1) (2000) 1–7.
[31] J.A. Moreto, D.B. Villarino de Castro, L.D.O. Bueno, H.D.A. Ponte, Equivalence between hot tensile and creep testing data for Kanthal A1 alloy, REM-REVISTA ESCOLA DE MINAS 64 (2005) (2011) 181–186.
[32] D.J. Inforzato, G.F. Batalha, E.F. Prados, L. d. O. Bueno, Equivalence Between Hot Tensile and Creep Data in Aluminum Alloy Al7475-T7351. Part 1: Relations Involving Stress, Strain Rate and Temperature, in: 69th ABM International Annual Congress, São Paulo, 2014, pp. 8310–8322.
[33] E. Charkaluk, A. Bignonnet, A. Constantinescu, K. Dang Van, Fatigue design of structures under thermomechanical loadings, Fatigue Fract. Eng. Mater. Struct. 25 (12) (2002) 1199–1206.
[34] X. Wu, G. Quan, R. MacNeil, Z. Zhang, X. Liu, C. Sloss, Thermomechanical Fatigue of Ductile Cast Iron and Its Life Prediction, Metall. Mater. Trans. A 46 (6) (2015) 2530–2543.
[35] U.W. Cho, W.N. Findley, Creep and plastic strains of 304 stainless steel at 593C under step stress changes, considering aging, J. Appl. Mech. Trans. ASME 49 (2) (1982) 297–304.
[36] W. Chen, F. Wang, M. Feng, Study of a modified non-unified model for time-dependent behavior of metal materials, Mech. Mater. 113 (2017) 69–76.
[37] F. Szmytka, L. Rémy, H. Maitournam, A. Köster, M. Bourgeois, New flow rules in elasto-viscoplastic constitutive models for spheroidal graphite cast-iron, Int. J. Plast. 26 (6) (2010) 905–924.
[38] G. Kang, Q. Kan, Constitutive modeling for uniaxial time-dependent ratcheting of SS304 stainless steel, Mech. Mater. 39 (5) (2007) 488–499.
[39] Z.L. Zhan, J. Tong, A study of cyclic plasticity and viscoplasticity in a new nickel-based superalloy using unified constitutive equations. Part I: Evaluation and determination of material parameters, Mech. Mater. 39 (1) (2007) 64–72.
[40] K. Ho, A unified constitutive law for cyclic viscoplasticity, Int. J. Solids Struct. 46 (5) (2009) 1007–1018.
[41] M. Becker, H.P. Hackenberg, A constitutive model for rate dependent and rate independent inelasticity. Application to IN718, Int. J. Plast. 27 (4) (2011) 596–619.
[42] P. Perzyna, Thermodynamic Theory of Viscoplasticity, Adv. Appl. Mech. 11 (1971) 313–354.
[43] J. Lubliner, On the structure of the rate equations of materials with internal variables, Acta Mech. 17 (1–2) (1973) 109–119.
[44] J.L. Chaboche, G. Rousselier, On the plastic and viscoplastic constitutive equations-part I: Rules developed with internal variable concept, J. Pressure Vessel Technol. Trans. ASME 105 (2) (1983) 153–158.
[45] A.D. Freed, J.L. Chaboche, K.P. Walker, A viscoplastic theory with thermodynamic considerations, Acta Mech. 90 (1–4) (1991) 155–174.
[46] J.L. Chaboche, A review of some plasticity and viscoplasticity constitutive theories, Int. J. Plast. 24 (10) (2008) 1642–1693.
[47] B. Larsson, B. Storåkers, A state variable interpretation of some rate-dependent inelastic properties of steel, J. Eng. Mater. Technol. 100 (4) (1978) 395–401.
[48] K. Ikegami, Y. Nitsu, Effect of creep prestrain on subsequent plastic deformation, Int. J. Plast. 1 (1985) 331–345.
[49] Y. Ohashi, M. Kawai, T. Momose, Effects of Cyclic Plasticity on Subsequent Creep for Type 316 Stainless Steel at Elevated Temperature, J. Eng. Mater. Technol. 108 (1) (1986) 68–74.
[50] T.H. Alden, Strain hardening during low temperature creep of 304 stainless steel, Acta Metall. 35 (11) (1987) 2621–2626.
[51] A.D. Freed, K.P. Walker, Viscoplasticity with creep and plasticity bounds, Int. J. Plast. 9 (2) (1993) 213–242.
[52] M. Rieth, A. Falkenstein, P. Graf, S. Heger, U. Jäntsch, M. Klimiankou, E. Materna-Morris, H. Zimmermann, Creep of the austenitic steel AISI 316 L (N) – Experiments and Models. FZKA 7065, Tech. rep., Forschungszentrum Karlsruhe in der Helmholtz-Gemeinschaft, Karlsruhe (2004).
[53] A. Palacios, M.E. Navarro, Z. Jiang, A. Avila, G. Qiao, E. Mura, Y. Ding, High-temperature corrosion behaviour of metal alloys in commercial molten salts, Sol. Energy 201 (2020) 437–452.
[54] J.M. Delimont, M.K. Murdock, W.F. Ng, S.V. Ekkad, Effect of temperature on microparticle rebound characteristics at constant impact velocity - Part II, J. Eng. Gas Turbines Power 137 (11) (2015).
[55] M. Ekström, S. Jonsson, High-temperature mechanical- and fatigue properties of cast alloys intended for use in exhaust manifolds, Mater. Sci. Eng., A 616 (2014) 78–87.
[56] ISO, Metallic materials - Tensile testing - Part 2: Method of test at elevated temperature (2011).
[57] ISO, Metallic materials – Tensile testing – Part 1: Method of test at room temperature (2016).
[58] M. Calmunger, G. Chai, S. Johansson, J. Moverare, Deformation behaviour in advanced heat resistant materials during slow strain rate testing at elevated temperature, Theoret. Appl. Mech. Lett. 4 (4) (2014) 041004.
[59] ISO, Corrosion of metals and alloys – Stress corrosion testing – Part 7: Method for slow strain rate testing (2005).
[60] ASTM, Standard test methods for stress relaxation for materials and structures (2008).
[61] J.H. Laflen, C.E. Jaske, Cyclic Relaxation Response Under Creep-Fatigue Conditions, Stress Relaxation Testing. ASTM International (1979).
[62] S.C. Bose, K. Singh, J. Swaminathan, D.S. Sarma, S.C. Bose, K. Singh, J. Swaminathan, D.S. Sarma, Prediction of creep life of X10CrMoVNbN-91 (P-91) steel through short term stress relaxation test methodology, Mater. Sci. Technol. 20 (10) (2004) 1290–1296.
[63] A. Pagliarello, J. Beddoes, The stress relaxation and creep behaviour of a manganese-stabilized austenitic stainless steel, J. Strain Anal. Eng. Des. 44 (3) (2009) 201–209.
[64] J. Beddoes, T. Mohammadi, Comparison of stress relaxation and creep strain rates for the superalloy IN738LC, J. Strain Anal. Eng. Des. 45 (8) (2010) 587–592.
[65] J. Beddoes, Prediction of creep properties for two nickel-base superalloys from stress relaxation testing, J. Strain Anal. Eng. Des. 46 (6) (2011) 416–427.
[66] Y. Wang, M. Spindler, C. Truman, D. Smith, Critical analysis of the prediction of stress relaxation from forward creep of Type 316H austenitic stainless steel, Mater. Des. 95 (2016) 656–668.
[67] ASTM, Standard Test Method for Measurement of Fatigue Crack Growth Rates (2014).
[68] M. Calmunger, G. Chai, R. Eriksson, S. Johansson, J.J. Moverare, Characterization of Austenitic Stainless Steels Deformed at Elevated Temperature, Metall. Mater. Trans. A 48 (10) (2017) 4525–4538.
[69] S.Y. Lee, C. Takushima, J. ichi Hamada, N. Nakada, Macroscopic and microscopic characterizations of Portevin-LeChatelier effect in austenitic stainless steel using high-temperature digital image correlation analysis, Acta Mater. 205 (2021) 116560.

[70] F.D. León-Cázares, F. Monni, T. Jackson, E.I. Galindo-Nava, C.M. Rae, Stress response and microstructural evolution of nickel-based superalloys during low cycle fatigue: Physics-based modelling of cyclic hardening and softening, Int. J. Plast. 128 (January 2020) 102682.
[71] A. Malekan, M. Farvizi, S.E. Mirsalehi, N. Saito, K. Nakashima, Holding time influence on creep behavior of transient liquid phase bonded joints of Hastelloy X, Mater. Sci. Eng. A 772(August 2019) (2020) 138694.
[72] D.G. Morris, Creep 316 Stainless, Acta Metall. 26 (7) (1978) 1143–1151.
[73] J.C. Zhao, M. Larsen, V. Ravikumar, Phase precipitation and time-temperature-transformation diagram of Hastelloy X, Mater. Sci. Eng., A 293 (1) (2000) 112–119.
[74] A.F. Padilha, D.M. Escriba, E. Materna-Morris, M. Rieth, M. Klimenkov, Precipitation in AISI 316L(N) during creep tests at 550 and 600 C up to 10 years, J. Nucl. Mater. 362 (1) (2007) 132–138.
[75] C.P. Cheng, T.S. Lui, L.H. Che, A study of the 500 to 900C tensile deformation behaviour of spheroidal graphite cast iro, Cast Metals 8 (4) (1996) 211–216.
[76] M. Aghaie-Khafri, N. Golarzi, Forming behavior and workability of Hastelloy X superalloy during hot deformation, Mater. Sci. Eng., A 486 (1–2) (2008) 641–647.
[77] S. Mitra, D. McLean, Work hardening and recovery in creep, Proc. Roy. Soc. Lond. Ser. A. Math. Phys. Sci. 295 (1442) (1966) 288–299.
[78] J. Gittus, Development of a theoretical equation for steady-state dislocation creep and comparison with data, Acta Metall. 22 (6) (1974) 789–791.